NeuroImage 211 (2020) 116615

Contents lists available at ScienceDirect

NeuroImage

journal homepage: www.elsevier.com/locate/neuroimage

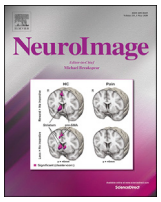

Frontoparietal theta-gamma interactions track working memory enhancement with training and tDCS

Kevin T. Jones [a,b,1], Elizabeth L. Johnson [c,d,1], Marian E. Berryhill [a,*]

[a] University of Nevada-Reno, Department of Psychology, Cognitive and Brain Sciences, Reno, NV, 89557, USA
[b] University of California-San Francisco, Department of Neurology, Neuroscape, San Francisco, CA, 94158, USA
[c] University of California-Berkeley, Helen Wills Neuroscience Institute, Berkeley, CA, 94720, USA
[d] Wayne State University, Institute of Gerontology, Life-Span Cognitive Neuroscience Program, Detroit, MI, 48202, USA

ARTICLE INFO

Keywords:
Cognitive training
Cross-frequency coupling
Neurostimulation
Prefrontal cortex
Working memory

ABSTRACT

Despite considerable interest in enhancing, preserving, and rehabilitating working memory (WM), efforts to elicit sustained behavioral improvements have been met with limited success. Here, we paired WM training with transcranial direct current stimulation (tDCS) to the frontoparietal network over four days. Active tDCS enhanced WM performance by modulating interactions between frontoparietal theta oscillations and gamma activity, as measured by pre- and post-training high-density electroencephalography (EEG). Increased phase-amplitude coupling (PAC) between the prefrontal stimulation site and temporo-parietal gamma activity explained behavioral improvements, and was most effective when gamma occurred near the prefrontal theta peak. These results demonstrate for the first time that tDCS-linked WM training elicits lasting changes in behavior by optimizing the oscillatory substrates of prefrontal control.

1. Introduction

Working memory (WM), the mental workspace in which information is maintained and manipulated, is capacity-limited to ~4 items (Cowan, 2001). As the foundation of successful cognitive performance, it is understandable that WM improvement is sought through training (Morrison and Chein, 2011; von Bastian and Oberauer, 2014; Berryhill, 2017). Yet, WM resists reliable, generalized improvement. Studies of cognitive training are plagued with mixed results and report little to no transfer of training gains (Morrison and Chein, 2011; Sala and Gobet, 2017; Nguyen et al., 2019; Schwaighofer et al., 2015). Augmenting WM training with noninvasive neurostimulation, such as transcranial direct current stimulation (tDCS), has shown promise in enhancing behavioral outcomes beyond training alone (Berryhill, 2017). Noninvasive neurostimulation techniques such as tDCS modulate the resting potentials of underlying neuronal populations (Nitsche and Paulus, 2001; Stagg and Nitsche, 2011; Nitsche et al., 2008) and are thought to facilitate neuroplasticity (Filmer et al., 2014). Specifically, tDCS interacts with multiple neurotransmitters and neuromodulators (Stagg and Nitsche, 2011) and increases the hemodynamic response within stimulated regions (Jones et al., 2015; Muthalib et al., 2018). In addition to these physiological effects, recent research reports that tDCS also affects neural oscillations (Luft et al., 2018; Reinhart et al., 2015), and enhances both functional and resting state connectivity (Kunze et al., 2016; Mangia et al., 2014; Park et al., 2013). However, the absence of a mechanistic account of tDCS-linked performance gains remains a critical gap in knowledge.

Here, we used high-density electroencephalography (EEG) combined with current modeling to investigate how four sessions of WM training paired with frontoparietal tDCS improved young adults' WM. Previous analysis revealed that active tDCS strengthened the task-relevant frontoparietal network, as demonstrated by increased theta (4–8 Hz) connectivity and alpha desynchronization compared to sham stimulation (Jones et al., 2017). Indeed, our initial report is one of many linking cognitive performance to coordinated theta activity across spatial scales (Alekseichuk et al., 2017; Hsu et al., 2017; Polania et al., 2012; Reinhart et al., 2017; Anguera et al., 2013; Solomon et al., 2017; Johnson et al., 2017). In contrast, cross-frequency coupling between theta oscillations and gamma (>30 Hz) activity permits information transfer across *temporal* (and spatiotemporal) scales during cognitive tasks (Bonnefond et al., 2017; Canolty and Knight, 2010; Helfrich and Knight, 2016). Theta-gamma phase-amplitude coupling (PAC) increases with WM load (Axmacher et al., 2010; Leszczynski et al., 2015), supports stimulus

* Corresponding author. Department of Psychology (296), 1664 N. Virginia Street Reno, NV, 89557, USA.
E-mail address: mberryhill@unr.edu (M.E. Berryhill).
[1] Denotes equal contribution.

https://doi.org/10.1016/j.neuroimage.2020.116615
Received 14 December 2019; Received in revised form 14 January 2020; Accepted 5 February 2020
Available online 7 February 2020

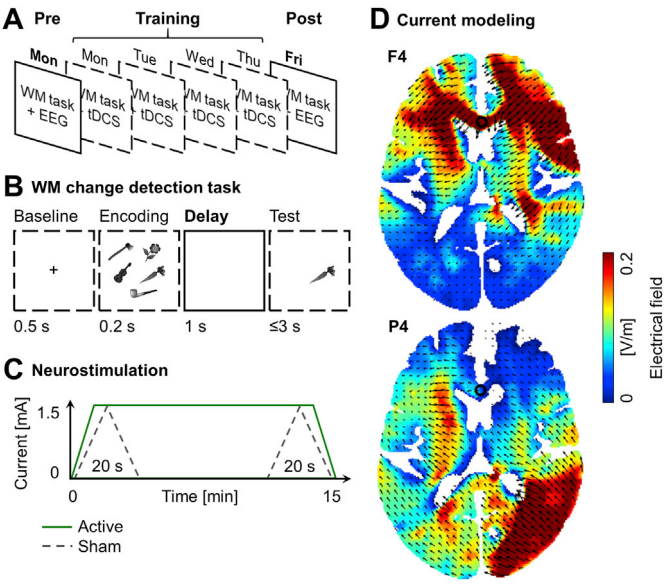

Fig. 1. Participants completed four WM training sessions with active or sham tDCS.

(**A**) WM training. Training took place over four sessions (Monday-Thursday) following tDCS. Participants completed the pre- and post-training sessions during high-density EEG collection without tDCS (Monday and Friday). Bold, data analyzed.

(**B**) WM task. Five grayscale items appeared (200 ms) followed by a delay (1000 ms) and an old/new change detection recognition probe. Bold, data analyzed.

(**C**) TDCS protocol. Active anodal stimulation was applied continuously for 15 min and sham stimulation was applied for 20 s at the beginning and end of 15 min. Green, active; gray, sham.

(**D**) Electrical field changes following tDCS. 1.5 mA tDCS was applied with the anode positioned at F4 (top) or P4 (bottom) and cathode at the contralateral cheek. Anode position alternated over the 4 days of training.

processing (Johnson et al., 2018; Daume et al., 2017), and carries information about perceptual and mnemonic representations (Heusser et al., 2016; Watrous et al., 2015). These findings corroborate theta-gamma PAC as a neurophysiological signature of WM.

Recent studies report changes in both theta-gamma PAC and WM performance acutely following transcranial alternating current stimulation (tACS; Hanslmayr et al., 2019). In addition to increasing the strength of PAC in temporal regions (Reinhart and Nguyen, 2019), tACS-linked WM benefits were shown to be maximal when gamma tACS was applied at the peak of the theta wave (i.e., phase-dependent coding; Alekseichuk et al., 2016). These findings suggest that both the strength and timing of theta-gamma interactions might track WM performance gains. Despite the central role of PAC in WM, only one study has investigated whether WM training might elicit sustained changes in PAC — and it was conducted in children. That study reported increased PAC between frontoparietal alpha-beta oscillations and left temporal gamma activity (Barnes et al., 2016). There are no reports in adults of PAC and behavioral improvement with cognitive training or tDCS.

In the present study, we hypothesized that augmenting WM training with tDCS would shift both the strength and timing of theta-gamma PAC and that changes in PAC would track an individual's performance gains. To test this hypothesis, we re-analyzed data from a double-blind, sham-controlled, within-subjects training study in healthy young adults with frontoparietal tDCS and pre- and post-training high-density EEG (Jones et al., 2017). We chose to use this dataset given the documented WM and frontoparietal theta connectivity benefits following training with active, but not sham, tDCS. The task's high trial count (n = 432) and difficulty further ensured both stable EEG data on the individual level and high numbers of correct and incorrect trials, permitting investigation of individual subsequent memory (SM) effects. Here, we examined PAC between frontoparietal theta oscillations, frequency-tuned to individual brain dynamics (Reinhart and Nguyen, 2019), and whole-brain gamma activity. All PAC data were subjected to two-tiered statistical testing, permitting dual assessment of the influence of (1) *individual* PAC on WM (regardless of tDCS group), and (2) tDCS *group* (active, sham) on PAC. We anticipated that active tDCS paired with WM training, beyond WM training alone, would optimize PAC between the stimulated frontoparietal network and gamma activity, enhancing WM.

2. Materials and methods

2.1. Participants

Twenty-four right-handed University of Nevada students (mean ± SD, age: 24.20 ± 3.81 years) participated. The sample size was justified based on a power analysis which demonstrated that, for a correlation of 0.5 between individual PAC and WM performance (regardless of tDCS group), a sample of 20 participants achieves 80% power (alpha = 0.05, two-tailed) (Faul et al., 2009). Participants were randomly assigned tDCS group membership (females: active/sham: 5/6). Participants were screened for use of neuroleptic, hypnotic, and seizure medications, and reported no history of neurological disorders or brain injury. Data for one participant from the active tDCS group were excluded due to excessive noise in the pre-training EEG. The University of Nevada Institutional Review Board approved all procedures. Participants provided informed consent and were compensated $15/hour ($70 total).

2.2. WM training

Participants first completed a WM change detection task while high-density EEG was recorded, prior to WM training or tDCS (pre-training session; Fig. 1A). The same day (Monday), the EEG cap was removed, and participants received tDCS before performing the WM task a second time (offline stimulation). On days 2–4 (Tuesday-Thursday), participants received tDCS and then completed the WM change detection task. During the final session (Friday), participants completed the WM change detection task during high-density EEG recording, but without tDCS (post-training session).

Each WM change detection trial began with a central fixation point (500 ms) followed by 5 grayscale pictures of common objects (200 ms) drawn from a set of 20 items (ant, axe, carrot, chicken, corn, fence, flower, football, eyeglasses, hammer, kettle, kite, leaf, pipe, scissors, snake, squirrel, toothbrush, windmill, violin) presented in 5 of 9 pseudorandom locations (3.5 × 3.5°; Fig. 1B). A blank delay (1000 ms) was followed by a recognition probe. Participants made an old/new judgment (3000-ms limit) indicating whether the probe item was encoded in the same location (50% each; Snodgrass and Vanderwart, 1980). The inter-trial interval was jittered between 1000 and 1500 ms. Participants completed 432 trials per session. Trials were coded as correct (i.e., hits, correct rejections) or incorrect (misses, false alarms).

2.3. Neurostimulation

2.3.1. TDCS protocol

Stimulation consisted of a single continuous direct current delivered by a battery-driven stimulator (Eldith MagStim, GmbH, Ilmenau, Germany). Current (1.5 mA, 15 min) was delivered through two 5 × 7 cm^2 electrodes within saline-dampened sponges (Fig. 1C). Sham stimulation included 20 s of ramping the stimulation up and down at the beginning and end of the 15-min period to provide the physical sensation of stimulation associated with current change. Participants and experimenters were double-blinded to the tDCS condition. Participants completed a post-tDCS questionnaire to report adverse symptoms; no participants reported any nor indicated they were aware of the stimulation condition, consistent with other research groups (Reinhart et al., 2017).

The anode location alternated by session between the right prefrontal cortex (PFC; F4, International 10–20 System) and posterior parietal

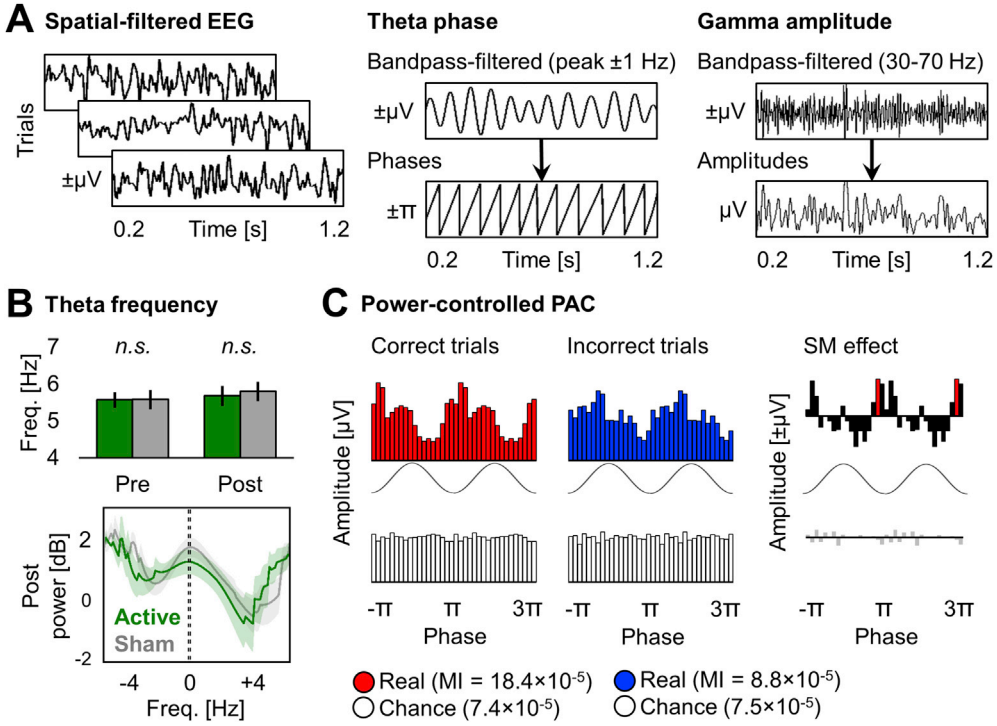

Fig. 2. Theta-gamma interactions were computed from the pre- and post-training EEG.

A) Spectral decomposition. EEG data were spatial-filtered and segmented into 1000-ms delay trials (left), and then separately filtered at peak theta (middle) and broadband gamma (right) frequencies. Theta phase and gamma amplitude time series were extracted using the Hilbert transform.

B) Peak theta detection. There was a peak in the theta band in every participant, with no differences in peak frequency between tDCS groups (top). Post-training power spectra were aligned to individual peak frequencies for display (bottom). Green, active; gray, sham; error bars and shading, SEM.

C) Computation of theta-gamma interactions. Phase-amplitude distributions were constructed separately from 50 correct and 50 incorrect trials (top, left and middle; 100 iterations; 2 cycles shown for clarity). The MI was obtained by measuring the divergence of the observed distribution from the uniform distribution. SM strength was calculated by subtracting the incorrect MI from the correct MI (here, $18.4–8.8 \times 10^{-5} = 9.6 \times 10^{-5}$). SM phase was calculated as the phase of maximal difference when subtracting the incorrect distribution from the correct distribution (top, right; marked in red). SM strength was validated by recomputing the chance MI from the same 50 trials with amplitudes permuted (bottom; 1000 iterations). Red, real correct data; blue, real incorrect data; white, same data with permuted amplitudes.

cortex (PPC; P4) in counterbalanced order (P4–F4–P4–F4 or F4–P4–F4–P4). The cathode was placed on the contralateral cheek for both montages (Jones et al., 2014, 2015, 2017; Jones, 2015; Elmer et al., 2009; Jones and Berryhill, 2012; Stephens and Berryhill, 2016; Reinhart and Woodman, 2015). We used this F4/P4 alternating approach based on the results of a previous longitudinal WM training study in older adults (Jones, 2015). In that study, although all three active tDCS montages were linked to statistically significant training and transfer benefits as compared to sham stimulation, the alternating F4/P4 montage elicited the greatest *numerical* benefits. Thus, we sought to delineate the EEG correlates of tDCS-linked WM training gains following a single neurostimulation protocol that yields benefits in both younger and older adults (Jones, 2015; Jones et al., 2017).

2.3.2. Current modeling

Current modeling was performed using the Realistic vOlumetric Approach to Simulate Transcranial Electric Stimulation (ROAST) software to map electrical field changes throughout the brain (Huang et al., 2018). ROAST is an open-source MATLAB-based, automated pipeline that applies SPM8 segmentation to the head and neck. Following segmentation, typical isotropic electrical conductivities are assigned to the tissues and electrodes, typical boundary conditions are assigned to the surfaces, and simulation of current flow is achieved by solving the Laplace equation (Reinhart et al., 2017):

$$\nabla \cdot (\sigma \nabla V) = 0 \quad (1)$$

where V is potential and σ is conductivity. Current modeling was conducted for the two anode locations (F4, P4) on the MNI-152 standard head (Grabner et al., 2006) and the cathode on the contralateral cheek (Fig. 1D).

2.4. High-density EEG

2.4.1. Data acquisition and preprocessing

EEG was recorded in DC mode at a sampling rate of 1000 Hz with a vertex (Cz) reference from 256 high-impedance electrodes. Electrodes were mounted in a HydroCel Geodesic Sensor Net amplified by a Net Amps 300 amplifier and acquired using Net Station 4.5.5 software (Electrical Geodesics Inc., Eugene, OR) running on a 2.7 GHz dual-core Apple Power Mac G5. Electrode impedances were kept below 50 KΩ.

Raw EEG data were passed through a 0.5–100 Hz two-pass Butterworth infinite impulse response (IIR) bandpass filter and 60-Hz line noise was removed using discrete Fourier transform. The outputs were manually inspected to reject channels displaying artifactual signal (e.g., from poor contact), then down-sampled to 250 Hz and segmented into 3-s trials (−1 to +2 s from the onset of each sample array). Independent components analysis (ICA) was performed on good channels to remove artifacts (i.e., electrooculogram and microsaccadic movements, auricular components, heartbeat, and residual cranial muscle activity; Hipp and Siegel, 2013). Channels positioned over the face, ears, and neck were discarded, and any rejected channels were replaced via interpolation of the mean of the nearest neighboring channels (7.4 channels on average). The remaining 194 channels were manually re-inspected blind to task parameters to reject trials containing residual noise, and the surface Laplacian spatial filter was applied to minimize volume conduction and increase the robustness of the signal source (Cohen, 2015; Perrin et al., 1989; He et al., 2018; Lai et al., 2018). All clean trials were analyzed; mean correct + incorrect, active pre-training: 293 + 139 (SD: 16), active post-training: 314 + 118 (17), sham pre-training: 277 + 156 (48), and sham post-training: 286 + 145 (42). Preprocessing routines were performed using custom-built MATLAB (MathWorks, Natick, MA) scripts with Fieldtrip software (Oostenveld et al., 2011).

2.4.2. Oscillatory peak detection

The 500-ms baseline and 1000-ms delay data segments were zero-padded to 10 s and multiplied with a Hanning taper, and power of 2–10 Hz (0.1-Hz resolution, 2-Hz bandwidth) was computed using a fast Fourier transform approach (Helfrich et al., 2018). Power spectra were averaged across trials. Delay power spectra were then log-transformed on the pre-stimulus baseline to remove 1/f background activity and reveal oscillatory components induced by the WM task. Individual corrected power spectra were averaged across all channels and oscillatory peaks were defined as the frequency of maximal prominence from the Gaussian distribution (Haegens et al., 2014). We repeated this analysis using only frontoparietal seed channels (described in Section 2.4.3) and note that outputs did not differ between approaches ($t(1,45) < 1.6$).

2.4.3. Cross-frequency analysis

Phase-amplitude distributions were quantified from the 1000-ms delay epochs per the modulation index (MI) method (Fig. 2; Tort et al., 2010). First, the event-related potential (ERP) was subtracted from each data segment separately for correct and incorrect trials to ensure that input data signals were not contaminated by simultaneous voltage shifts across frequencies or channels (Johnson et al., 2017, 2018; Aru et al., 2015). The outputs were zero-padded to 10 s, and separately bandpass-filtered at the individual peak theta frequency (2-Hz bandwidth) and broadband gamma frequency (30–70 Hz) using two-pass Butterworth IIR filters, ensuring a narrowband modulatory frequency and sufficiently broadband amplitude frequency (Aru et al., 2015; Dvorak and Fenton, 2014). Next, the phase time series were calculated from the theta signal and the amplitude time series were calculated from the gamma signal using the Hilbert transform. Phase time series were calculated for the frontoparietal seed channels ipsilateral (F4, P4) and contralateral (F3, P3) to anodal stimulation. Amplitude time series were calculated for all channels. Using a bootstrapping approach, PAC was computed between each phase seed time series and all amplitude time series (Johnson et al., 2018; Barnes et al., 2016; Maris et al., 2011; van der Meij et al., 2012; Friese et al., 2013).

To achieve stable, power-controlled estimates of PAC per individual, we randomly selected 50 correct trials and 50 incorrect trials so that all PAC calculations were performed on the same length of input data (Tort et al., 2010). Notably, 50 s of data is well over the recommended minimum of 10 s and approximates the MI obtained from all theta cycles (Dvorak and Fenton, 2014). This step was repeated 100 times to sample all correct and incorrect trials with equal power (i.e., 50 s of data, 100 iterations). For each set of 50 trials, the instantaneous phase values were pooled and divided into 18 bins and the analytic amplitude envelope was averaged and normalized per phase bin. Phase-amplitude distributions were then averaged across all iterations. The MI (i.e., strength of amplitude modulation) was calculated from the mean phase-amplitude distribution as the Fisher's Z-transformed Kullback-Leibler divergence:

$$MI = \frac{1}{2}\ln\left(\frac{1 + D(P,Q)}{1 - D(P,Q)}\right) \quad (2)$$

where D (P,Q) is defined as:

$$D(P,Q) = \sum P * \log\left[\frac{P}{Q}\right] \quad (3)$$

where D is Kullback-Leibler divergence, P is the observed distribution, and Q is the uniform distribution. We utilized the MI method because it allows for the pooling of non-continuous data segments into one distribution (Tort et al., 2010). This makes it well-suited to robustly estimate PAC over short epochs provided one epoch contains multiple cycles of the low-frequency oscillation (Aru et al., 2015).

Because we were interested in the neural mechanisms behind WM success, PAC data were first indexed by SM, an approach borrowed from the long-term memory literature (Paller and Wagner, 2002). To determine SM strength, we subtracted the incorrect MI from the correct MI (Fig. 2C, top left and middle). To determine phase coding of SM, we subtracted the incorrect distribution from the correct distribution and detected the phase of maximal difference (Fig. 2C, top right, marked in red). This approach reveals the coupling strength and phase features which precede a correct compared to incorrect behavioral response, with positive values (i.e., correct > incorrect) reflecting successful WM formation.

2.4.4. Validation against oscillatory power

Because differences in power at the modulatory frequency can confound phase estimates and elicit spurious PAC (Aru et al., 2015; Canolty et al., 2006; Cole and Voytek, 2017; Gerber et al., 2016; Jensen et al., 2016), we first validated SM strength and phase data against theta SM power data at each seed channel. The 500-ms baseline and 1000-ms delay epochs were filtered at the individual peak theta frequency and the amplitude time series were calculated using the Hilbert transform and squared to produce power. Delay power time series were then corrected on the pre-stimulus baseline (i.e., (delay – baseline mean)/baseline mean) and averaged over the 1000-ms epoch to reveal task induced activity (Jones et al., 2017). To determine SM power, we subtracted the mean incorrect power from the mean correct power at each of the four frontoparietal seed channels. The PAC SM strength and phase data were averaged across the whole brain and correlated with SM power using Spearman's rank correlation (SM strength × SM power; Fig. S1) and circular-linear correlation (SM phase × SM power; Fig. S2). Correlations were thresholded at $p < 0.05$, uncorrected. Circular statistics were performed using the CircStat toolbox (Berens, 2009).

2.4.5. Validation against permuted data

The SM strength effects were separately validated by comparison against chance effects generated from the analysis of permuted time series (Fig. 2C, bottom). This procedure controls for any statistical regularities between correct and incorrect trials in the original input data, such as differences in band-limited theta or gamma activity, or in noise contributing to spurious PAC (Axmacher et al., 2010; Tort et al., 2010; Aru et al., 2015; Dvorak and Fenton, 2014; Canolty et al., 2006; Cole and Voytek, 2017; Gerber et al., 2016; Jensen et al., 2016). For each phase bin, the amplitudes were randomly permuted across pooled trials and the MI was re-computed. This was repeated 10 times per iteration on the same randomly selected 50 trials as the original data (1000 iterations total) and then averaged across all iterations. This procedure shuffles the timing of the amplitude envelope relative to the phase without altering the phase time series or any other aspect of the original data, thereby estimating the MI that would be expected solely by chance. If regularities exist in the data which are not related to the temporal coordination between theta and gamma signals, then they will be present in the validation data.

2.4.6. Statistics

Group-level statistical analyses of SM strength and phase were performed using non-parametric tests on the whole brain and corrected for multiple comparisons using cluster-based permutation tests (Maris and Oostenveld, 2007). Clusters were formed in space by thresholding correlations (ρ) or chi-square ranks (χ^2) at $p < 0.05$ using the maximum size criterion. Permutation distributions were then generated by randomly shuffling labels (i.e., per-subject WM performance or tDCS group; 1000 iterations) and corrected p-values were obtained by comparing the observed data to the random permutation distributions. This is an extremely powerful approach because it recreates any biases in the data with each randomization and thus tests for effects without any assumption over where they may occur.

Data were first submitted to correlation testing to analyze the relationship between individual PAC and post-training WM performance, regardless of tDCS group ($n = 23$). SM strength data were tested using Spearman's rank correlation, a non-linear measure that does not assume

normal distribution, and SM phase data were tested using circular-linear correlation. The cluster-corrected correlation masks (Figs. 3A, 4A, 5A and 6A) were used to index individual data for visualizing significant brain-behavior relationships (Figs. 3B, 4B, 5B and 6B). Data were then submitted to independent-samples testing between groups to analyze the effect of tDCS group on PAC (n = 11 active, 12 sham). SM strength data were analyzed using the Kruskal-Wallis test (i.e., non-parametric ANOVA), a measure of independence between distributions, and SM phase data were analyzed using the equivalent test for circular data (cmtest.m). Circular statistics were performed using the CircStat toolbox (Berens, 2009).

Interpretation was based on three criteria. First, to confirm that SM strength effects were due to PAC rather than other statistical regularities between correct and incorrect trials, we submitted the amplitude-permuted validation data to the same correlation and between-groups tests as the real data. Any observation of overlapping effects obtained from submitting real versus amplitude-permuted data to the same statistical test would preclude interpretation of effects as being due to PAC. The correlation masks obtained using real data (Figs. 3A and 4A) were used to index individual amplitude-permuted data to emphasize the difference in brain-behavior relationships observed using real data versus those that would be expected by chance (Figs. 3B and 4B). Second, to assess whether training with active tDCS improved task performance by way of affecting PAC, we compared the masks obtained from correlation testing (Figs. 3A, 4A, 5A and 6A; S3A and C; S4A and C) to those obtained from between-groups testing (Figs. 3C, 4C, 5C and 6C; S3B and D; S4B and D). Third, to confirm that tDCS group effects were due to training with active versus sham tDCS and not any other regular variation that may have existed between groups, we compared the masks obtained from between-groups testing at the pre-versus post-training session. The post-training correlation masks (Figs. 3A, 4A, 5A and 6A) were used to index individual pre-training data to visualize training effects associated with active versus sham tDCS (Figs. 3D, 4D, 5D and 6D).

Finally, we quantified tDCS-linked training changes using the Cohen's d measure of effect size (i.e., (active mean pre-post change – sham mean pre-post change)/pooled pre-training SD; Morris, 2008). This analysis indicates the size of the pre-post training × tDCS interactive effect on PAC correlates of WM performance, controlling for pre-training variability. Together, these analysis steps yield a conservative approach to test the hypothesis that augmenting training with tDCS optimizes theta-gamma PAC, enhancing WM.

3. Results

3.1. TDCS-linked WM training improves WM

As previously described (Jones et al., 2017), four days of WM training paired with frontoparietal tDCS improved WM performance (i.e., proportion correct) significantly more than training alone (2 session (pre-, post-training) × 2 group (active, sham tDCS) ANOVA, $F(1,21) = 4.35$, $p = 0.049$, partial $\eta^2 = 0.17$, Greenhouse-Geisser corrected). The interaction reflected the significant group difference at the post-training session (mean ± SD, active: 0.76 ± 0.05, sham: 0.70 ± 0.07; $t(19.76) = 2.07$, $p = 0.05$, equal variances not assumed), that was not present pre-training (active: 0.70 ± 0.05, sham: 0.69 ± 0.09; $t(17.19) = 0.29$, $p = 0.77$). Only the active tDCS group showed training-related task improvement ($t(10) = 3.12$, $p = 0.01$); the sham group did not improve ($t(11) = 0.85$, $p = 0.41$). There was a main effect of session ($F(1,21) = 9.46$, $p = 0.006$, partial $\eta^2 = 0.31$, Greenhouse-Geisser corrected), but not of group ($F(1, 21) = 1.42$, $p = 0.25$). Behavioral effects were observed 24 h after the final WM training + tDCS session.

3.2. Frontoparietal tDCS reaches frontoparietal cortex

Current modeling confirmed that the neurostimulation applied during WM training maximally affected targeted sites at alternating ends of the frontoparietal network (Fig. 1D). Anodal stimulation of right PFC (F4) altered the electrical field in right PFC and, to a lesser extent, in frontopolar, orbitofrontal, ventral temporal, and left frontal regions. Anodal stimulation of right PPC (P4) altered the electrical field in right PPC and, to a lesser extent, in occipital and ventral temporal regions.

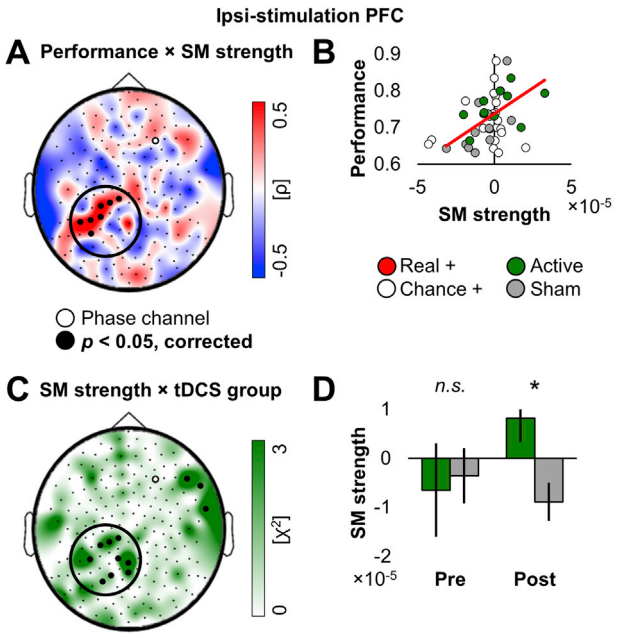

Fig. 3. Theta-gamma PAC between the stimulated PFC and posterior sites tracked WM training gains.

A) Superior performers showed greater PAC between theta at the PFC stimulation site (F4, marked in white) and left-central gamma amplitudes (marked in black) during WM formation. Cluster-corrected correlation between SM strength (correct MI – incorrect MI) and task performance at the post-training session, regardless of tDCS group. White circle, phase seed channel; black circles, amplitude channels that showed significant effects.

B) The greater the SM effect, the better the performance. The relationship between SM strength and WM performance at the channels marked in (**A**). Green, real active data; gray, real sham data; white, same data with permuted amplitudes; red, fit.

C) Active tDCS altered SM strength at a subset of channels in (**A**). Cluster-corrected between-groups test on SM strength at the post-training session, same conventions as (**A**).

D) Active tDCS increased the SM effect, increasing performance (pre-post interaction Cohen's d = 0.793). Mean SM strength by tDCS group at the pre- and post-training sessions at the channels marked in (**A**). Overlapping correlation and between-groups effects were specific to the post-training session. Green, real active data; gray, real sham data; error bars, SEM; *, significant.

3.3. Theta-gamma interactions

To test the hypothesis that theta-gamma PAC tracked *individual* WM training gains, we computed stable, power-controlled phase-amplitude distributions per the MI method (Tort et al., 2010). We calculated phase-amplitude distributions between individually-determined theta phase time series at the frontoparietal seeds (tDCS sites: F4, P4; contralateral homologues: F3, P3) and broadband gamma amplitude time series at all channels (Johnson et al., 2018; Barnes et al., 2016; Maris et al., 2011; van der Meij et al., 2012; Friese et al., 2013), and then extracted the coupling strength and phase features preceding correct compared to incorrect responses (Fig. 2). This resulted in four whole-brain PAC SM profiles per participant, per session.

Individual peak theta frequency was equal across tDCS groups (pre-training: mean ± SD, active: 5.6 ± 0.7 Hz, sham: 5.6 ± 0.9 Hz; $t(20.35) = 0.05$, $p = 0.96$; post-training: active: 5.7 ± 0.9 Hz, sham: 5.8 ± 0.9 Hz; $t(20.85) = 0.33$, $p = 0.75$; Fig. 2B). To control for spurious effects, we

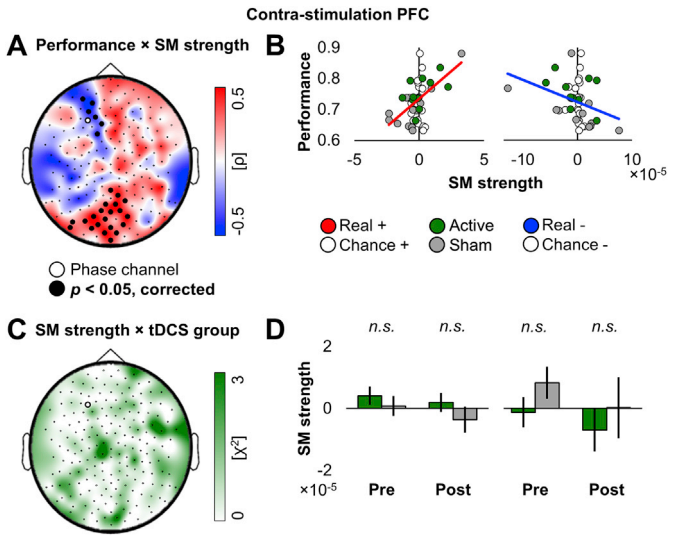

Fig. 4. Theta-gamma PAC from the contralateral PFC did not differ between tDCS groups.
(**A**) Superior performers showed both greater PAC between theta at the contralateral PFC site (F3, marked in white) and posterior gamma amplitudes (marked in black) and less PAC within the contralateral PFC site during WM formation. Cluster-corrected correlation between SM strength and task performance at the post-training session, regardless of tDCS group. White circle, phase seed channel; black circles, amplitude channels that showed significant effects.
(**B**) Bimodal SM effects for performance. The relationships between SM strength and WM performance at the channels marked in (**A**). Lines were fit separately to the channels exhibiting positive (left) and negative (right) brain-behavior relationships. Green, real active data; gray, real sham data; white, same data with permuted amplitudes; red, fit of real positive effect; blue, fit of real negative effect.
(**C**) There were no effects of tDCS group. Cluster-corrected between-groups test on SM strength at the post-training session, same conventions as (**A**).
(**D**) Mean SM strength by tDCS group at the pre- and post-training sessions at the channels marked in (**A**), separated by the direction of the relationship as in (**B**). Green, real active data; gray, real sham data; error bars, SEM.

ruled out any statistical dependency between theta power and theta-derived coupling strength and phase data at the frontoparietal seeds (Axmacher et al., 2010; Tort et al., 2010; Aru et al., 2015; Canolty et al., 2006). This analysis confirmed that theta power did not correlate with coupling strength or phase outcomes (Figs. S1–S2; $p > 0.05$, uncorrected). Neither were there significant effects of tDCS group on theta power (Jones et al., 2017).

To investigate the relationship between individual theta-gamma interactions and behavior, across all subjects *regardless* of tDCS group, whole-brain PAC SM data were first correlated with WM performance at the post-training session. Only then did we test for differences between active and sham tDCS groups. We attributed statistically significant effects to training + tDCS when there was: (1) overlap in correlation and between-groups effects post-training, and (2) no between-groups effect pre-training. Pre-post training × tDCS interaction effect sizes were then quantified by means of Cohen's d to show the extent to which tDCS induced *changes* in PAC with training, beyond training alone. The effects were further validated against amplitude-permuted chance data to control for any differences afforded correct versus incorrect trials that were not due to temporal coordination between theta oscillations and gamma activity (Fig. 2C; Axmacher et al., 2010; Tort et al., 2010; Aru et al., 2015; Canolty et al., 2006).

3.3.1. TDCS enhances coupling strength for WM at the stimulated PFC

We first tested whether coupling strength (i.e., SM strength = correct MI – incorrect MI; Fig. 2C) between theta oscillations at the PFC stimulation site (F4) and whole-brain gamma activity correlated with WM performance during the post-training session. Significant clusters in the left-central topography reveal a *positive* relationship between SM strength and WM performance (Fig. 3A; mean $\rho = 0.482$, $p = 0.012$). To visualize this relationship, we averaged individuals' SM strength data across significant channels, plotted it against their behavior, and fit a line to the data post hoc. Individuals with overall superior performance exhibited greater PAC between PFC theta and posterior gamma on correct compared to incorrect trials (i.e., SM strength > 0; Fig. 3B). There were no significant brain-behavior relationships using chance data (mean $\rho = -0.002$, $p = 1$), confirming that these effects were due to temporal coordination between theta oscillations at the stimulated PFC and posterior gamma activity.

Testing of the same whole-brain SM strength data by tDCS group returned multiple significant clusters showing predominant overlap in left-central topography (Fig. 3C; mean $\chi^2 = 3.529$, $p = 0.028$; pre-post interaction Cohen's $d = 0.793$). Between-groups effects mirrored the brain-behavior relationships (Fig. 3D), revealing that training + tDCS increased PAC between PFC theta and posterior gamma preceding successful behavioral responses, partially explaining behavioral training gains in the active tDCS group. Critically, there were no overlapping between-groups effects when tested using pre-training data (mean $\chi^2 = 0.653$, $p = 1$) or chance data (mean $\chi^2 = 0.332$, $p = 1$). Thus, training with active tDCS enhanced temporal coordination between PFC theta oscillations and posterior gamma activity.

To further characterize the influence of WM training paired with tDCS on PAC outside stimulated areas, we submitted the SM strength data calculated from theta oscillations at the PFC seed contralateral to anodal stimulation (F3) to the same analyses. Correlation testing of the post-training data returned multiple significant positive *and* negative clusters (Fig. 4A; positive mean $\rho = 0.383$, $p = 0.006$; negative mean $\rho = -0.376$, $p = 0.048$), revealing bimodal effects and opposite patterns of WM success in better versus worse performers. Notably, superior performance was linked to two patterns: (1) greater PAC between left PFC theta and posterior gamma on correct compared to incorrect trials, and (2) less theta-gamma PAC within left PFC (Fig. 4B; chance positive mean $\rho = 0.004$, negative mean $\rho = -0.015$, $p = 1$). However, testing the same data between groups returned no significant clusters (Fig. 4C–D; $p = 1$), suggesting that tDCS effects were restricted to theta oscillations in the stimulated frontoparietal network.

Finally, we submitted the SM strength data calculated from theta oscillations at the PPC seeds (P4, P3) to the same set of analyses. Correlation testing of the post-training data at the PPC stimulation site returned a negative cluster in the left-central topography (Fig. S3A; mean $\rho = -0.477$, $p = 0.002$), indicating that decreased PAC was associated with superior performance. However, there were no significant effects between tDCS groups (Fig. S3B; $p = 0.584$). Correlation testing of the post-training data at the PPC site contralateral to anodal stimulation returned a positive cluster over posterior regions (Fig. S3C; mean $\rho = 0.359$, $p = 0.008$), but no significant between-groups effects (Fig. S3D; $p = 0.894$). There were no significant PPC brain-behavior relationships when tested using chance data (P4 mean $\rho = -0.047$, P3 mean $\rho = 0.006$, $p = 1$). These inconsistent PPC results isolate the beneficial effects of tDCS on theta-gamma coupling strength to PFC.

In summary, at the post-training session, WM success was linked to greater PAC between PFC theta oscillations and gamma activity in posterior regions. In the same individuals, greater PAC within left PFC preceded WM failures, revealing a double dissociation. Behavioral training gains were maximal when there was greater PAC between PFC theta and posterior gamma *and* less PAC within left PFC during WM formation. TDCS selectively enhanced this beneficial coupling between theta oscillations in the stimulated PFC and temporo-parietal gamma activity.

3.3.2. TDCS enhances phase coding for WM at the stimulated PFC

We next examined the contribution of phase coding, the timing of gamma activity to frontoparietal theta oscillations (i.e., SM phase = phase of peak difference, correct distribution – incorrect distribution; Fig. 2C, right), to WM performance during the post-training session. SM

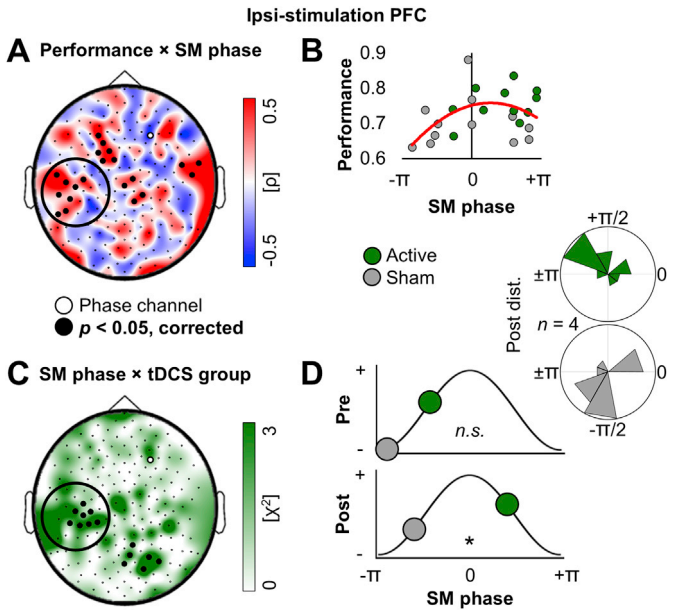

Fig. 5. Theta-gamma phase coding between the stimulated PFC and distributed sites tracked WM training gains.

A) Superior performers showed phase coding between theta at the PFC stimulation site (F4, marked in white) and distributed gamma amplitudes (marked in black) during WM formation. Cluster-corrected correlation between SM phase (phase of peak difference, correct distribution – incorrect distribution) and task performance at the post-training session, regardless of tDCS group. White circle, phase seed channel; black circles, amplitude channels that showed significant effects.

B) The closer gamma occurred to the falling flank, near the peak of the theta wave, the better the performance. The relationship between SM phase and WM performance at the channels marked in (**A**). A quadratic line was fit to the data to show phase-dependent coding for behavior. Green, real active data; gray, real sham data; red, fit.

C) Active tDCS adjusted phase coding at a subset of channels in (**A**). Cluster-corrected between-groups test on SM phase at the post-training session, same conventions as (**A**).

D) Active tDCS adjusted gamma toward the falling flank, near the peak of the theta wave, increasing performance (pre-post interaction Cohen's d = 0.621). Mean SM phase by tDCS group at the pre- and post-training sessions at the channels marked in both (**A**) and (**B**) on a schematic theta wave (standard cosine). Overlapping correlation and between-groups effects were specific to the post-training session. Inset: histograms of the preferred phase for SM at the post-training session. Green, real active data; gray, real sham data; *, significant.

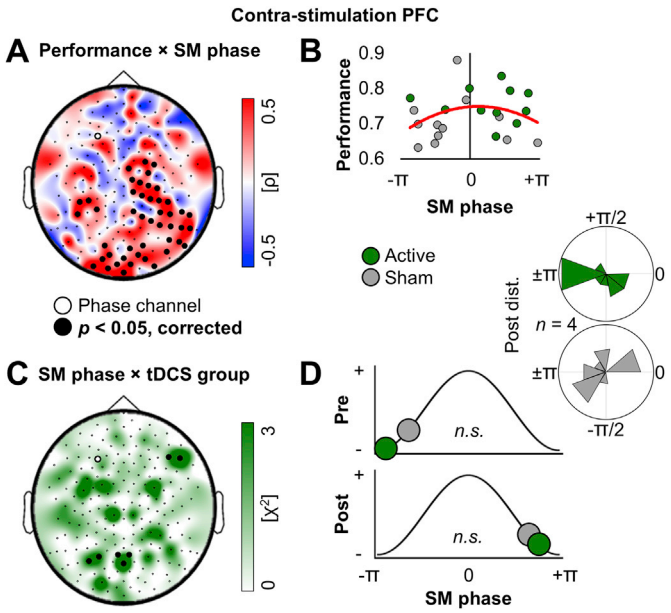

Fig. 6. Theta-gamma phase coding from the contralateral PFC did not differ between tDCS groups.

A) Superior performers showed phase coding between theta at the contralateral PFC site (F3, marked in white) and widespread gamma amplitudes (marked in black) during WM formation. Cluster-corrected correlation between SM phase and task performance at the post-training session, regardless of tDCS group. White circle, phase seed channel; black circles, amplitude channels that showed significant effects.

B) SM effects for performance. The relationship between SM phase and WM performance at the channels marked in (**A**). Green, real active data; dark gray, real sham data; red, fit.

C) There were no overlapping correlation and between-groups effects. Cluster-corrected between-groups test on SM phase at the post-training session, same conventions as (**A**). There were no overlapping correlation and between-groups effects.

D) Mean SM phase by tDCS group at the pre- and post-training sessions at the channels marked in (**A**) on a schematic theta wave (standard cosine). Inset: histograms of the preferred phase for SM at the post-training session. Green, real active data; gray, real sham data.

phase data were submitted to the same set of analyses as the SM strength data, using the equivalent circular statistical tests (Berens, 2009), to determine whether WM training + tDCS also affected phase coding specific to theta oscillations at the stimulated PFC.

Correlation testing of post-training SM phase at the PFC seed ipsilateral to anodal stimulation (F4) returned multiple significant clusters across a distributed topography (Fig. 5A; mean $\rho = 0.457$, $p = 0.022$). During successful WM, gamma on the falling flank near the peak of the PFC theta wave correlated with superior performance overall (Fig. 5B). Testing the same whole-brain SM phase data by tDCS group returned multiple significant clusters (Fig. 5C; mean $\chi^2 = 3.023$, $p = 0.027$; pre-post interaction Cohen's d = 0.621). Between-groups effects mirrored brain-behavior relationships in the left-central topography (Fig. 5D). Training + tDCS improved performance by tuning the timing of gamma activity relative to PFC theta oscillations. Critically, the pre-training data show no significant between-groups effects ($p = 1$). Thus, these between-groups effects were due to training paired with active tDCS.

To further characterize the influence of WM training paired with tDCS on phase coding, we next examined SM phase data calculated from the PFC seed contralateral to anodal stimulation (F3). Correlation testing of the post-training data returned multiple significant clusters across a widespread topography (Fig. 6A; mean $\rho = 0.445$, $p = 0.007$). During successful WM, gamma closer to the peak of the theta oscillation was associated with superior performance overall (Fig. 6B). However, testing the same data between groups returned no significant clusters (Fig. 6C–D; $p = 0.592$). This supports the interpretation that the effects of tDCS were specific to theta oscillations in the stimulated frontoparietal network.

Finally, we examined SM phase data calculated from theta oscillations at the PPC seeds (P4, P3). Correlation testing of the post-training data at the PPC stimulation site returned multiple significant clusters (Fig. S4A; mean $\rho = 0.442$, $p = 0.036$). However, testing the same data between groups identified no significant clusters (Fig. S4B; $p = 0.499$). Testing the post-training data at the contralateral PPC seed revealed no significant correlations (Fig. S4C; $p > 0.07$) and sparse between-groups effects (Fig. S4D). These null PPC results isolate the effects of tDCS on phase-dependent coding to theta oscillations at the stimulated PFC.

In summary, at the post-training session, WM performance was associated with phase-dependent coding of SM between PFC theta oscillations and widespread posterior gamma activity. Behavioral training gains were maximal when gamma activity associated with successful performance occurred on the falling flank near the peak of PFC theta waves. TDCS selectively enhanced this beneficial phase coding between theta oscillations at the stimulated PFC and temporo-parietal gamma activity.

4. Discussion

This study is the first to investigate the link between cross-frequency coupling and behavioral outcomes following WM training or tDCS in adults. We show that shifts in cross-frequency interactions between theta oscillations in the frontoparietal network and gamma activity tracked individual training gains. Specifically, superior performance was associated with greater PAC between PFC theta oscillations and posterior gamma activity *and* less PAC within left PFC during WM formation after training. Inferior performance was associated with the opposite pattern, revealing a double dissociation in the locus of theta-gamma interactions between participants who did and did not benefit from training. We further show that augmenting training with tDCS enhanced behavior by optimizing both the strength and timing of theta-gamma interactions, specifically between the stimulated PFC and temporo-parietal regions.

These findings fit proposals that PFC exerts top-down control over representations stored in posterior cortical regions, supporting cognitive performance (Friese et al., 2013). Indeed, neural oscillations are the purported mechanism for PFC control over posterior regions (Helfrich and Knight, 2016; de Vries et al., 2020); we provide critical evidence directly linking such oscillatory mechanisms to individual behavioral outcomes. We further demonstrate that behavioral change emerges from shifting the oscillatory mechanisms of PFC control. We propose a novel explanation of behavioral enhancement based on fine-tuning the oscillatory mechanisms of PFC control over posterior regions.

WM training gains, albeit modest at 5% improvement on the group level, were exclusive to the active tDCS group (Jones et al., 2017). For this reason, we evaluated this proposal by testing whether tDCS shifted theta-gamma interactions in the direction associated with superior performance. Behaviorally-relevant effects of tDCS were specific to the modulation of gamma activity by theta oscillations at the stimulated PFC. First, WM training + tDCS selectively increased the strength of coupling between theta oscillations at the stimulated PFC and temporo-parietal gamma activity. Second, WM training + tDCS selectively adjusted the timing of temporo-parietal gamma activity toward the peak of theta oscillations at the stimulated PFC. Both phenomena were specific to the stimulated PFC as no such patterns were observed at the contralateral PFC. Third, PPC effects were sparse and inconsistent, isolating behaviorally-relevant effects to PFC. We conclude that frontoparietal tDCS optimized both the strength and timing of theta-gamma interactions between the stimulated PFC and temporo-parietal regions, explaining WM training gains.

These findings are consistent with the sole report of WM training and PAC, which likewise indicated behavioral gains specific to left temporal gamma activity in children (Barnes et al., 2016). Here, left PFC correlates of WM performance illuminated gamma activity across widespread parieto-occipital regions and were unaffected by right-hemisphere tDCS. In contrast, anodal tDCS to the right frontoparietal network affected PAC and phase coding between right-PFC theta oscillations and left temporo-parietal gamma activity, enhancing performance. These converging results show that tDCS-linked WM training not only increases coordination across spatial scales within the stimulated network (Jones et al., 2017), but also across temporal scales selectively between the stimulated network and left temporo-parietal regions. This interpretation corroborates that of other reports based on co-occurring band-limited theta and cross-frequency theta-gamma interactions (Reinhart and Nguyen, 2019; Alekseichuk et al., 2016), permitting coordination across both spatial and temporal scales in the service of WM.

Understanding the mechanisms by which paired training and neurostimulation affects performance is critical for reliable, real-world applications. We provide insight regarding *how* a four-day training program improved WM performance. As previously described (Jones et al., 2017), the generalizability of our findings is limited by the sample size, and selection of a single task and neurostimulation protocol. That said, a sample of 20–30 healthy young adults is typical of EEG/MEG studies using homogenous samples, e.g., (Daume et al., 2017; Heusser et al., 2016; Friese et al., 2013), and the present study relied on individual brain-behavior relationships based on hundreds of trials per participant (Smith and Little, 2018). The present findings support the view that some aspects of disordered behavior may be altered by adjusting neural oscillations (Salimpour and Anderson, 2019). Specifically, theta-gamma PAC is reduced in the mildly cognitively impaired and further reduced in those with Alzheimer's disease compared to healthy other adults (Goodman et al., 2018). A recent report indicated that restoring theta-gamma PAC in temporal regions improved older adults' WM acutely following neurostimulation (Reinhart and Nguyen, 2019). We demonstrate that augmenting training with neurostimulation can elicit *sustained* changes in theta-gamma PAC, enhancing behavior. Future research should investigate the durability of such changes across a range of healthy and clinical populations.

4.1. Conclusion

Pairing frontoparietal tDCS with WM training improved behavior by optimizing the oscillatory mechanisms of PFC control. TDCS optimized the strength and timing of theta-gamma PAC between the stimulated PFC and left temporo-parietal regions, thus linking behavioral gains to coordination across spatiotemporal scales between the stimulated PFC and left temporo-parietal regions. In short, it is possible to elicit lasting changes in both brain and behavior by way of cognitive training. Here, changes in theta-gamma interactions persisted for at least 24 h post-training, consistent with the acute effects of directly entraining neural oscillations (Hanslmayr et al., 2019; Reinhart and Nguyen, 2019). Future studies are needed to investigate the durability of training-related changes in PAC across a range of populations and the extent to which these changes transfer to untrained tasks.

Declaration of competing interest

None.

CRediT authorship contribution statement

Kevin T. Jones: Conceptualization, Methodology, Formal analysis, Investigation, Writing - original draft, Writing - review & editing, Visualization. **Elizabeth L. Johnson:** Conceptualization, Methodology, Software, Validation, Formal analysis, Writing - original draft, Writing - review & editing, Visualization. **Marian E. Berryhill:** Conceptualization, Methodology, Resources, Writing - review & editing, Visualization, Supervision, Project administration, Funding acquisition.

Acknowledgements

We would like to thank Dr. Kara Blacker, Dr. Dwight Peterson, Dr. Robert Knight, Dr. Noa Ofen, and Gabriella Dimotsantos. The work was funded by the National Science Foundation (OIA 1632738 and 1632849 to MEB). EEG facilities are supported by the National Institutes of Health (NIGMS COBRE P20GM103650). Funding sources had no role in the study design; collection, analysis and interpretation of data; writing of the report; or decision to submit the article for publication.

Appendix A. Supplementary data

Supplementary data to this article can be found online at https://doi.org/10.1016/j.neuroimage.2020.116615.

References

Alekseichuk, I., et al., 2016. Spatial working memory in humans depends on theta and high gamma synchronization in the prefrontal cortex. Curr. Biol. 26 (12), 1513–1521.
Alekseichuk, I., et al., 2017. Intrahemispheric theta rhythm desynchronization impairs working memory. Restor. Neurol. Neurosci. 35 (2), 147–158.

Anguera, J.A., et al., 2013. Video game training enhances cognitive control in older adults. Nature 501 (7465), 97–101.
Aru, J., et al., 2015. Untangling cross-frequency coupling in neuroscience. Curr. Opin. Neurobiol. 31, 51–61.
Axmacher, N., et al., 2010. Cross-frequency coupling supports multi-item working memory in the human hippocampus. Proc. Natl. Acad. Sci. U. S. A. 107 (7), 3228–3233.
Barnes, J.J., et al., 2016. Training working memory in childhood enhances coupling between frontoparietal control network and task-related regions. J. Neurosci. 36 (34), 9001–9011.
Berens, P., 2009. CircStat: a MATLAB toolbox for circular statistics. J. Stat. Software 31 (10), 1–21.
Berryhill, M.E., 2017. Longitudinal tDCS: consistency across working memory training studies. Aims Neurosci. 4 (2), 71–86.
Bonnefond, M., Kastner, S., Jensen, O., 2017. Communication between Brain Areas Based on Nested Oscillations. eNeuro.
Canolty, R.T., Knight, R.T., 2010. The functional role of cross-frequency coupling. Trends Cognit. Sci. 14 (11), 506–515.
Canolty, R.T., et al., 2006. High gamma power is phase-locked to theta oscillations in human neocortex. Science 313 (5793), 1626–1628.
Cohen, M.X., 2015. Comparison of different spatial transformations applied to EEG data: a case study of error processing. Int. J. Psychophysiol. 97 (3), 245–257.
Cole, S.R., Voytek, B., 2017. Brain oscillations and the importance of waveform shape. Trends Cognit. Sci. 21 (2), 137–149.
Cowan, N., 2001. The magical number 4 in short-term memory: a reconsideration of mental storage capacity (vol 23, pg 87, 2001). Behav. Brain Sci. 24 (3).
Daume, J., et al., 2017. Phase-amplitude coupling and long-range phase synchronization reveal frontotemporal interactions during visual working memory. J. Neurosci. 37 (2), 313–322.
de Vries, I.E.J., Slagter, H.A., Olivers, C.N.L., 20202020. Oscillatory control over representational states in working memory. Trends Cognit. Sci. 24 (2), 150–162.
Dvorak, D., Fenton, A.A., 2014. Toward a proper estimation of phase-amplitude coupling in neural oscillations. J. Neurosci. Methods 225, 42–56.
Elmer, S., et al., 2009. Direct current induced short-term modulation of the left dorsolateral prefrontal cortex while learning auditory presented nouns. Behav. Brain Funct. 5, 29.
Faul, F., et al., 2009. Statistical power analyses using G*Power 3.1: tests for correlation and regression analyses. Behav. Res. Methods 41 (4), 1149–1160.
Filmer, H.L., Dux, P.E., Mattingley, J.B., 2014. Applications of transcranial direct current stimulation for understanding brain function. Trends Neurosci. 37 (12), 742–753.
Friese, U., et al., 2013. Successful memory encoding is associated with increased cross-frequency coupling between frontal theta and posterior gamma oscillations in human scalp-recorded EEG. Neuroimage 66, 642–647.
Gerber, E.M., et al., 2016. Non-sinusoidal activity can produce cross-frequency coupling in cortical signals in the absence of functional interaction between neural sources. PloS One 11 (12).
Goodman, M.S., et al., 2018. Theta-gamma coupling and working memory in alzheimer's dementia and mild cognitive impairment. Front. Aging Neurosci. 10, 101.
Grabner, G., et al., 2006. Symmetric atlasing and model based segmentation: an application to the hippocampus in older adults. Med Image Comput Comput Assist Interv 9 (Pt 2), 58–66.
Haegens, S., et al., 2014. Inter- and intra-individual variability in alpha peak frequency. Neuroimage 92, 46–55.
Hanslmayr, S., Axmacher, N., Inman, C.S., 2019. Modulating human memory via entrainment of brain oscillations. Trends Neurosci. 42 (7), 485–499.
He, B., et al., 2018. Electrophysiological source imaging: a noninvasive window to brain dynamics. Annu. Rev. Biomed. Eng. 20, 171–196.
Helfrich, R.F., Knight, R.T., 2016. Oscillatory dynamics of prefrontal cognitive control. Trends Cognit. Sci. 20 (12), 916–930.
Helfrich, R.F., et al., 2018. Neural mechanisms of sustained attention are rhythmic. Neuron 99 (4), 854–865 e5.
Heusser, A.C., et al., 2016. Episodic sequence memory is supported by a theta-gamma phase code. Nat. Neurosci. 19 (10), 1374–+.
Hipp, J.F., Siegel, M., 2013. Dissociating neuronal gamma-band activity from cranial and ocular muscle activity in EEG. Front. Hum. Neurosci. 7, 338.
Hsu, W.Y., et al., 2017. Enhancement of multitasking performance and neural oscillations by transcranial alternating current stimulation. PloS One 12 (5), e0178579.
Huang, Y., et al., 2018. ROAST: an open-source, fully-automated, realistic volumetric-approach-based simulator for TES. Conf Proc IEEE Eng Med Biol Soc 3072–3075, 2018:
Jensen, O., Spaak, E., Park, H., 2016. Discriminating valid from spurious indices of phase-amplitude coupling. eNeuro 3 (6).
Johnson, E.L., et al., 2018. Dynamic frontotemporal systems process space and time in working memory. PLoS Biol. 16 (3), e2004274.
Jones, K.T., et al., 2015. Longitudinal neurostimulation in older adults improves working memory. PloS One 10 (4), e0121904.
Jones, K.T., Berryhill, M.E., 2012. Parietal contributions to visual working memory depend on task difficulty. Front. Psychiatr. 3, 81.
Jones, K.T., Gozenman, F., Berryhill, M.E., 2014. Enhanced long-term memory encoding after parietal neurostimulation. Exp. Brain Res. 232 (12), 4043–4054.
Johnson, E.L., Dewar, C.D., Solbakk, A.-K., Endestad, T., Meling, T.R., Knight, R.T., 2017. Bidirectional frontoparietal oscillatory systems support working memory. Curr. Biol. 27 (12), 1829–1835.
Jones, K.T., Gozenman, F., Berryhill, M.E., 2015. The strategy and motivational influences on the beneficial effect of neurostimulation: a tDCS and fNIRS study. Neuroimage 105, 238–247.
Jones, K.T., Peterson, D.J., Blacker, K.J., Berryhill, M.E., 2017. Frontoparietal neurostimulation modulates working memory training benefits and oscillatory synchronization. Brain Res. 1667, 28–40.
Kunze, T., et al., 2016. Transcranial direct current stimulation changes resting state functional connectivity: a large-scale brain network modeling study. Neuroimage 140, 174–187.
Lai, M., et al., 2018. A comparison between scalp- and source-reconstructed EEG networks. Sci. Rep. 8 (1), 12269.
Leszczynski, M., Fell, J., Axmacher, N., 2015. Rhythmic working memory activation in the human Hippocampus. Cell Rep. 13 (6), 1272–1282.
Luft, C.D.B., Zioga, I., Bhattacharya, J., 2018. Anodal transcranial direct current stimulation (tDCS) boosts dominant brain oscillations. Brain Stimul 11 (3), 660–662.
Mangia, A.L., Pirini, M., Cappello, A., 2014. Transcranial direct current stimulation and power spectral parameters: a tDCS/EEG co-registration study. Front. Hum. Neurosci. 8, 601.
Maris, E., Oostenveld, R., 2007. Nonparametric statistical testing of EEG- and MEG-data. J. Neurosci. Methods 164 (1), 177–190.
Maris, E., van Vugt, M., Kahana, M., 2011. Spatially distributed patterns of oscillatory coupling between high-frequency amplitudes and low-frequency phases in human iEEG. Neuroimage 54 (2), 836–850.
Morris, S.B., 2008. Estimating effect sizes from pretest-posttest-control group designs. Organ. Res. Methods 11 (2), 364–386.
Morrison, A.B., Chein, J.M., 2011. Does working memory training work? The promise and challenges of enhancing cognition by training working memory. Psychon. Bull. Rev. 18 (1), 46–60.
Muthalib, M., et al., 2018. Focal hemodynamic responses in the stimulated hemisphere during high-definition transcranial direct current stimulation. Neuromodulation 21 (4), 348–354.
Nguyen, L., Murphy, K., Andrews, G., 2019. Immediate and long-term efficacy of executive functions cognitive training in older adults: a systematic review and meta-analysis. Psychol. Bull. 145 (7), 698–733.
Nitsche, M.A., Paulus, W., 2001. Sustained excitability elevations induced by transcranial DC motor cortex stimulation in humans. Neurology 57 (10), 1899–1901.
Nitsche, M.A., et al., 2008. Transcranial direct current stimulation: state of the art 2008. Brain Stimul 1 (3), 206–223.
Oostenveld, R., et al., 2011. FieldTrip: open source software for advanced analysis of MEG, EEG, and invasive electrophysiological data. Comput. Intell. Neurosci. 2011, 156869.
Paller, K.A., Wagner, A.D., 2002. Observing the transformation of experience into memory. Trends Cognit. Sci. 6 (2), 93–102.
Park, C.H., et al., 2013. Transcranial direct current stimulation increases resting state interhemispheric connectivity. Neurosci. Lett. 539, 7–10.
Perrin, F., et al., 1989. Spherical splines for scalp potential and current density mapping. Electroencephalogr. Clin. Neurophysiol. 72 (2), 184–187.
Polania, R., Paulus, W., Nitsche, M.A., 2012. Modulating cortico-striatal and thalamo-cortical functional connectivity with transcranial direct current stimulation. Hum. Brain Mapp. 33 (10), 2499–2508.
Reinhart, R.M.G., Nguyen, J.A., 2019. Working memory revived in older adults by synchronizing rhythmic brain circuits. Nat. Neurosci. 22, 820–827.
Reinhart, R.M., Woodman, G.F., 2015. Enhancing long-term memory with stimulation tunes visual attention in one trial. Proc. Natl. Acad. Sci. U. S. A. 112 (2), 625–630.
Reinhart, R.M., et al., 2015. Synchronizing theta oscillations with direct-current stimulation strengthens adaptive control in the human brain. Proc. Natl. Acad. Sci. U. S. A. 112 (30), 9448–9453.
Reinhart, R.M.G., et al., 2017. Using transcranial direct-current stimulation (tDCS) to understand cognitive processing. Atten. Percept. Psychophys. 79 (1), 3–23.
Sala, G., Gobet, F., 2017. Does far transfer exist? Negative evidence from chess, music, and working memory training. Curr. Dir. Psychol. Sci. 26 (6), 515–520.
Salimpour, Y., Anderson, W.S., 2019. Cross-frequency coupling based neuromodulation for treating neurological disorders. Front. Neurosci. 13 (125).
Schwaighofer, M., Fischer, F., Buhner, M., 2015. Does working memory training transfer? A meta-analysis including training conditions as moderators. Educ. Psychol. 50 (2), 138–166.
Smith, P.L., Little, D.R., 2018. Small is beautiful: in defense of the small-N design. Psychon. Bull. Rev. 25 (6), 2083–2101.
Snodgrass, J.G., Vanderwart, M., 1980. A standardized set of 260 pictures: norms for name agreement, image agreement, familiarity, and visual complexity. J Exp Psychol Hum Learn 6 (2), 174–215.
Solomon, E.A., et al., 2017. Widespread theta synchrony and high-frequency desynchronization underlies enhanced cognition. Nat. Commun. 8 (1), 1704.
Stagg, C.J., Nitsche, M.A., 2011. Physiological basis of transcranial direct current stimulation. Neuroscientist 17 (1), 37–53.
Stephens, J.A., Berryhill, M.E., 2016. Older adults improve on everyday tasks after working memory training and neurostimulation. Brain Stimul 9 (4), 553–559.
Tort, A.B., et al., 2010. Measuring phase-amplitude coupling between neuronal oscillations of different frequencies. J. Neurophysiol. 104 (2), 1195–1210.
van der Meij, R., Kahana, M., Maris, E., 2012. Phase-amplitude coupling in human electrocorticography is spatially distributed and phase diverse. J. Neurosci. 32 (1), 111–123.
von Bastian, C.C., Oberauer, K., 2014. Effects and mechanisms of working memory training: a review. Psychol. Res. 78 (6), 803–820.
Watrous, A.J., et al., 2015. Phase-amplitude Coupling Supports Phase Coding in Human ECoG, 4. Elife.